ELSEVIER

International Journal of Heat and Fluid Flow 23 (2002) 381–397

International Journal of HEAT AND FLUID FLOW

www.elsevier.com/locate/ijhff

Axisymmetric numerical simulations of turbulent flow in rotor stator enclosures

R. Jacques, P. Le Quéré *, O. Daube

LIMSI, BP 133, 91403 Orsay Cedex, France

Received 3 March 2001; accepted 16 December 2001

Abstract

We present axisymmetric numerical simulations of transitional and chaotic flow regimes in rotor–stator cavities of radial aspect ratio approximately 8. These simulations are carried out using a second order time and space accurate algorithm which integrates the axisymmetric unsteady Navier–Stokes equations in stream function-azimuthal vorticity-azimuthal velocity form. Detailed flow analysis has been carried out for selected values of the rotational Reynolds number (Re_θ) up to 10^6. At the largest value considered, computations have been performed using 4096 mesh points in the radial direction, which has required using a multi-domain decomposition algorithm implemented on a parallel machine. The limitations and consequences of the axisymmetry assumption are first discussed and checked against available experimental results. The evolutions of the instantaneous flow structure and of its first and second order statistic moments as the Reynolds number increases are discussed. It is shown that the dynamics of the flow mainly consists of travelling waves propagating in the stator and rotor boundary layers and of inertial waves in the core region, and that for moderate Reynolds numbers ($Re_\theta \simeq 3 \times 10^5$), the rotor boundary layer is almost completely steady while large amplitude fluctuations are found in the stator boundary layer. The evolution of second order moments confirms the fundamentally asymmetrical role of the boundary layers along the rotor and along the stator. A turbulent kinetic energy budget is shown which exhibits some specific features attributed to the rotation effects and to a lesser extent to the axisymmetry assumption. © 2002 Published by Elsevier Science Inc.

1. Introduction

Computation of turbulent flow between two differentially rotating disks is of considerable engineering interest. Many engineering configurations, such as the secondary cooling flows in turbomachines or the flows in the torque converter of an automatic gearbox, can be described by an enclosure of large radial aspect ratio bounded by one stationary disk (the stator) and another rotating about its axis of symmetry (the rotor). In such a configuration, the flow structure consists of the superposition of a primary azimuthal flow, which is driven by viscous shear, and a secondary flow in the cross section of the cavity due to rotation effects. This secondary flow generally consists of two boundary layers, one outward along the rotor and one inward along the stator. Depending on the values of the aspect ratio and Reynolds number, a core region of zero radial velocity rotating locally as a solid body can exist between both boundary layers. The radial distribution of this angular velocity in the core (equal to 0.313 for the laminar similarity solution) is thus of paramount engineering interest since it directly governs the radial pressure distribution and hence the axial forces on the disks. In most practical cases, these flows are, if not fully turbulent, at least largely transitional. It has long been recognized that both boundary layers have different stability properties, the rotor boundary layer being much more stable than that along the stator (Itoh et al., 1990). As a consequence there exist flows which are laminar in some regions of the cavity and turbulent in others. It has also been observed that the boundary conditions on the peripheral shroud and on the internal hub have an important influence, not only on the radial distribution of the azimuthal velocity but because they also directly affect the onset of transition and consequently the intensity of turbulence. In addition, fundamental studies have shown that rotation can significantly affect the

* Corresponding author. Tel.: +33-169-85-8080; fax: +33-169-85-8088.

E-mail address: plq@limsi.fr (P. Le Quéré).

0142-727X/02/$ - see front matter © 2002 Published by Elsevier Science Inc.
PII: S0142-727X(02)00137-6

Nomenclature

C_m	$= M/(1/2)\rho\Omega^2 R_2^5$, torque coefficient
G	$= H/R_2$, gap ratio
H	disks clearance
M	$= 2\pi \int \mu R^2 (\partial U_2/\partial Z)_{\text{wall}} \mathrm{d}R$, torque
R	radial location
R_1	internal radius (hub)
R_2	external radius (peripheral shroud)
Re_H	$= H^2\Omega/v$, Reynolds number
Re_θ	$= R_2^2\Omega/v$, rotational Reynolds number
Re_r	$= r^2\Omega/v$, local Reynolds number
U	radial velocity component
U_τ	$= \sqrt{\tau_w/\rho}$, wall frictional velocity
V	azimuthal velocity component
W	axial velocity component
Z	axial location
r	dimensionless radial location (R/H)
s	$= R_1/R_2$, radius ratio
u	dimensionless radial component of the velocity $(U_1/H\Omega)$
v	dimensionless azimuthal component of the velocity
w	dimensionless axial component of the velocity
y^+	$= Z(u_\tau/v)$, dimensionless wall coordinate
z	dimensionless axial location (Z/H)
Γ	boundary of the computational domain
Δ	mesh size
Ω	angular rotational velocity of the rotor
ϵ	viscous dissipation rate of the turbulent kinetic energy
κ	turbulent kinetic energy
η	Kolmogorov scale
θ	azimuthal coordinate
μ	kinematic viscosity
v	dynamic viscosity
ρ	density
τ_w	$= \mu(\partial U_\tau/\partial N)$, wall shear stress
ψ	stream function
ω	azimuthal component of the vorticity
$\partial/\partial N$	wall normal derivative

characteristics of turbulence, namely reduction of the dissipation rate of the turbulent kinetic energy (Cambon and Jacquin, 1989; Ibbetson and Tritton, 1975), increase of the anisotropy (Cambon and Jacquin, 1989) and strong reduction of the extension of the logarithmic wall region (Nagano et al., 1991).

All these specific features make accurate computations of these turbulent flows a formidable challenge. In particular, mixing length (Chew and Vaughan, 1988) and κ–ϵ turbulence models have been reported to produce unsatisfactory results (Randriamampianina et al., 1997), and the development of improved models has been an area of extensive research over the last few years. A review of most of these recent efforts is available in Iacovides and Launder (1995). Although improved predictions can be expected and are indeed obtained from Reynolds stress models (RSM), such as those developed to account for rotation (Elena and Schiestel, 1996), such computations are still very expensive, not mentioning numerical stability problems. Improved κ–ϵ models or algebraic stress models (ASM) can thus still represent a good compromise between accuracy and computational time (Iacovides and Launder, 1995; Ton and Lin, 1994) and detailed data are therefore needed in order to understand the origin of their alleged limitations.

Our initial aim was to perform direct numerical simulations (DNS) at large enough Reynolds numbers in order to contribute such data and establish reference solutions. Due to the simultaneous improvements in algorithms and computing resources, DNS has now become a powerful and reliable tool to investigate fluid flows in the transitional and turbulent regimes. The results not only give access to detailed information on the space and time evolution of the flow structures, which are of interest on their own, but can also help compute statistical moments of the flow quantities and characterize deviations from the mean quantities, information increasingly needed in engineering applications. DNS is, however, generally restricted to academic configurations, most of them consisting of one inhomogeneous direction coupled with 1 or 2 directions in which periodicity is assumed. In a pioneering contribution, Fromm (1987, 1988) performed simulations of rotor–stator flows using both the assumption of axisymmetry and of periodicity in the radial direction. He was able to show that even under these rather crude approximations the computations reproduced the instantaneous asymmetric behavior of the boundary layers on the rotor and on the stator after the onset of transition. In most rotor–stator configurations, the presence of the outer shroud strongly influences the flow and needs to be taken into account. Reaching the boundary layer regime of interest in the presence of a shroud leads one to consider cavities of relatively large radial aspect ratios, which turn out to be very computationally demanding, as also noted by Randriamampianina et al. (1997). As will be discussed later, reaching the largest rotational Reynolds number considered here has required a very large number of grid points in the (r, z) cross section plane, and carrying out

full 3D computations would have been barely feasible. We have thus decided to carry out computations under the axisymmetric assumption in order to reach Reynolds numbers corresponding to actual turbulent flows. We thus initially undertook these simulations in a geometry given to us [1] as an actual rotor–stator cavity. This cavity is characterized by the presence of an inner hub and extends from $R_1 > 0$ to R_2 in the radial direction, and both the inner hub and outer shroud are attached to the stator. In order to produce somewhat more general results, the computations were also extended for one given Reynolds number to a cavity extending from the axis of rotation to the same external radius, which corresponds exactly to the geometry investigated by Cheah et al. (1994).

In both cases, the computations were performed under the assumption of axisymmetry of the instantaneous flow. This assumption may obviously seem highly questionable and this point will be addressed in more detail in the second paragraph. Let us again point out here that this assumption was dictated by memory and cpu time limitations due to the huge number of grid points which would have been required to reach the highest value of the Reynolds number in the configuration considered here. Reaching asymptotic axisymmetric solutions and computing significant first, second and third order moments has required the equivalent of several thousands of cpu hours on a Cray C90 and a Cray T3E. We have recently started to extend these computations to 3D. Preliminary tests have been carried out for laminar flows just at the onset of unsteadiness. The results will be reported elsewhere. These tests have shown that extending to 3D the computations for the same range of Reynolds numbers as those considered here is hardly feasible at present. We nonetheless believe that the present axisymmetric computations, although they probably miss some key features of actual flows and cannot therefore claim to match quantitatively actual flow experiments, will prove helpful both at present for the insight they give into the flow dynamics and later as a reference to interpret 3D effects as 3D flow data become available.

This article is organized as follows. We present in the next section the geometrical configuration and recall the governing equations. The numerical algorithm used to perform the axisymmetric numerical simulations is described next. The numerical requirements are also addressed. The validity and consequences of the axisymmetry assumption are discussed next, first on the basis of scaling arguments and secondly by comparisons of our simulations against the experimental results of Cheah et al. (1994). The presentation of the results starts with a discussion of the evolution of the instantaneous space and time structure of the flow in the first configuration for the various Reynolds numbers investigated. We then discuss the evolution of the mean flow quantities and of their second order moments. A kinetic energy budget is shown next. Although in general agreement with those found in other types of flows, it does exhibit some specific features which should be reproduced by classical turbulence modelling. A detailed comparison of these results with those obtained from a κ–ϵ computation has been presented in Jacques et al. (1998).

2. Configuration and numerical algorithm

2.1. Configuration

We consider the flow of an incompressible newtonian fluid in a rotor–stator type cavity (see Fig. 1), whose lower horizontal plate rotates with angular velocity Ω. The clearance between the disks is H and these extend from R_1 to R_2 in the radial direction. Using the clearance H as the reference length, the computational domain reduces to the cross section $[R_1/H, R_2/H] \times [0, 1]$. The usual gap ratio G is defined as (H/R_2). For cavities which do not extend throughout to the rotation axis (i.e., $R_1 > 0$), complete definition of the geometry requires an additional parameter, the radius ratio s, which is defined as R_1/R_2. As stated in the introduction, we have considered two different geometries. The first one, hereafter referred to as CV1, is characterized by $G = 0.125$ and $s = 0.25$, and the second, referred to as CV2, is exactly the geometry considered in Cheah et al. (1994) and corresponds to $G = 0.127$ and $s = 0$ (Table 1). In both cavities the peripheral shroud is attached to the stator. In the first case, the inner hub is also assumed to be attached to the stator.

Under the assumption of axisymmetry, the dimensionless governing equations written in cylindrical coordinates with respect to a stationary frame reduce to

$$\begin{cases} \dfrac{\partial u}{\partial t} + u\dfrac{\partial u}{\partial r} + w\dfrac{\partial u}{\partial z} - \dfrac{v^2}{r} \\ \quad = -\dfrac{\partial p}{\partial r} + \dfrac{1}{Re_H}\left(\dfrac{1}{r}\dfrac{\partial}{\partial r}\left(r\dfrac{\partial u}{\partial r}\right) - \dfrac{u}{r^2} + \dfrac{\partial^2 u}{\partial z^2}\right) \\ \dfrac{\partial v}{\partial t} + u\dfrac{\partial v}{\partial r} + w\dfrac{\partial v}{\partial z} + \dfrac{uv}{r} = \dfrac{1}{Re_H}\left(\dfrac{1}{r}\dfrac{\partial}{\partial r}\left(r\dfrac{\partial v}{\partial r}\right) - \dfrac{v}{r^2} + \dfrac{\partial^2 v}{\partial z^2}\right) \\ \dfrac{\partial w}{\partial t} + u\dfrac{\partial w}{\partial r} + w\dfrac{\partial w}{\partial z} = -\dfrac{\partial p}{\partial z} + \dfrac{1}{Re_H}\left(\dfrac{1}{r}\dfrac{\partial}{\partial r}\left(r\dfrac{\partial w}{\partial r}\right) + \dfrac{\partial^2 w}{\partial z^2}\right) \\ \dfrac{1}{r}\dfrac{\partial ru}{\partial r} + \dfrac{\partial w}{\partial z} = 0 \end{cases} \tag{1}$$

where u, v, w are the radial, azimuthal and axial dimensionless velocity components, respectively, and P the pressure. These equations have been made dimensionless using H as reference length and ΩH as reference velocity. The Reynolds number which appears in the equations thus reads $Re_H = \Omega H^2/\nu$. It is customary to

[1] This work was carried out under a joint SNECMA-CNRS grant.

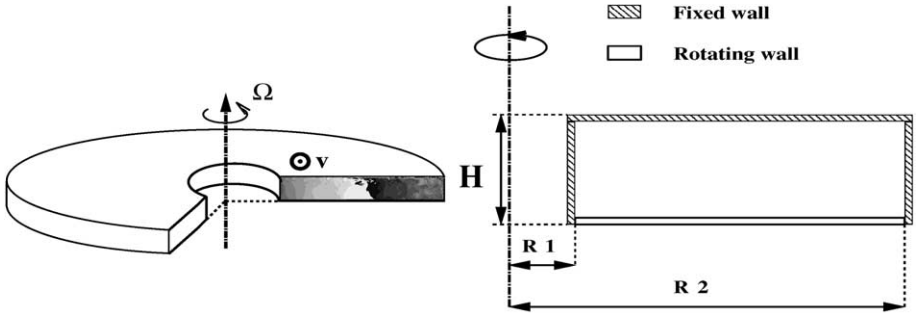

Fig. 1. Geometry.

Table 1
Geometric configurations parameters

Cavity	Gap ratio (G)	Radius ratio (s)
CV1	0.125	0.25
CV2 (Cheah)	0.127	0

present the results in terms of the usual rotational Reynolds number $Re_\theta = \Omega R_2^2/v$ and one has $Re_H = G^2 Re_\theta$.

2.2. Numerical algorithm

For these axisymmetric numerical simulations, the equations are cast into the alternative stream function (ψ), azimuthal vorticity (ω) and azimuthal velocity (v) formulation. The basic algorithm is described in Vanel et al. (1986) (see also Daube, 1992) and is only briefly recalled here. The time-stepping scheme combines an implicit treatment of the viscous terms and an explicit Adams–Bashforth extrapolation of the non-linear convective terms. Application of this time-stepping scheme yields an unsteady Stokes problem for the coupled variables (ψ, ω), and Helmholtz problem for the azimuthal velocity component v at each time step. These elliptic equations are supplemented with boundary conditions expressing the no-slip condition at the walls. Whereas the Helmholtz problem for v can be readily solved, the boundary conditions for the Stokes problem are $\psi|_\Gamma = 0$, $(\partial\psi/\partial n)|_\Gamma = 0$ which prevents the solution of these equations in a decoupled form. This problem is circumvented by the use of an influence matrix technique which allows one to determine the vorticity boundary values that ensure $(\partial\psi/\partial n)|_\Gamma = 0$. Solving the unsteady Stokes problem thus reduces to solving four elliptic problems. In total five Helmholtz problems have thus to be solved at each time step. Spatial discretization consists of a second order centered finite difference scheme. The three independent variables are discretized at the same locations $(i\Delta r, j\Delta z)$.

The Helmholtz solvers use partial diagonalization in the z direction, coupled to an LU direct decomposition in the radial direction. To port this algorithm on a parallel machine, a domain decomposition in the radial direction is implemented. It consists of an exact algebraic reorganization of the discrete Helmholtz problems which considers as primary variables the unknowns on the interfaces between the subdomains, and as secondary variables the unknowns in the subdomains. At each time step the discrete Helmholtz problems on the whole computational domain are solved exactly and directly using the Schur complement algorithm. Each subdomain is attached to an elementary processor. The communications between the processors are managed using the PVM library (Parallel Virtual Machine). We have used up to 64 processors and the communication time never exceeded 10% to the total elapsed time. Typical elapsed cpu time per point and time step was 1.5×10^{-6} s on a Cray T3D, and half of that on a T3E.

2.3. Numerical requirements

The numerical results that will be presented below are obtained with sufficiently fine mesh and time intervals to ensure that all the scales present in the flow are captured. This requires a priori estimates of these scales and a posteriori checks. Uniform spatial meshes were used in both spatial directions due to the recirculating nature of the flow, in which small structures can be found intermittently throughout the computational domain. The mesh size was determined a priori from estimates of the dissipation rate and confirmed a posteriori from the computed second order statistics. The a priori Kolmogorov scale η was in fact estimated on the Reynolds number Re_H and on the production of kinetic turbulent energy, assuming the existence of an equilibrium state $(\eta/H \approx 1.5 \times Re_H^{-4/5})$. It is also generally admitted that there must be at least three grid-points within the viscous sublayer (see e.g. Grötzbach, 1983) and that the mean grid size should not exceed $\pi \times \eta/H$. From the estimate of the wall friction velocity based on the sole azimuthal velocity component, the normal grid size must be on the order of: $\Delta z/H \leqslant \sqrt{5} Re_H^{-3/5}$. Satisfaction of this criterion leads to using 2049×129 grid points in the radial and axial direction for $Re_H = 5000$ $(Re_\theta = 3 \times 10^5)$ and 4097×513 for $Re_H = 15\,625$ $(Re_\theta = 10^6)$.

In both cases ($Re_H = 5000$ and $Re_H = 15625$), the first criterion ($\Delta = \sqrt{\Delta r \Delta z} \leqslant \pi \times \eta/H$) is satisfied with the above discretizations. It is thus believed that such spatial discretizations ensure accurate predictions of the smallest spatial scales encountered in the flow. The time resolution can also be a constraint and the allowable time steps, dictated by stability requirements, turn out to be smaller than an estimate of the Kolmogorov time scale ($\Omega \times t_\eta = 2.5 \times Re_H^{-3/5}$).

3. Discussion and consequences of axisymmetry assumption

As said in the introduction, the results which will be reported below were obtained under the assumption of axisymmetry of the instantaneous flow. The question then arises of the significance and usefulness of these results. It is indeed known that 2D numerical simulations miss some important phenomenological features of transitional and/or turbulent flows, such as bursting in a transitional boundary layer or in a pipe flow to name only two examples. Our preliminary fully 3D results obtained at lower Reynolds number have indeed shown that transition occurs earlier compared to the axisymmetric case. The energetics of 2D flows is also different since the energy cascade in 3D is replaced by an enstrophy cascade in 2D (see Lesieur, 1987). We however believe that, although our results could prove not to reproduce the actual phenomenology of transitional and/or turbulent rotor–stator flows, they could prove not as false as one could imagine a priori both for reasons based on scaling arguments and confirmed by comparisons with actual experiments.

Let us first point out that the assumption of axisymmetry of the instantaneous flow does not imply a null diagonal stress in the azimuthal direction (as would be the case in 2D planar flow). This azimuthal diagonal stress is indeed the largest of the diagonal stresses by almost an order of magnitude. Further, it is easily seen that the assumption of axisymmetry of the instantaneous flow does not bear on the production terms governing the growth of the velocity fluctuations (u', v', w') or of the Reynolds stresses. Indeed, the production tensor involves only gradients of this mean flow, which is axisymmetric, and thus reads

$$\mathscr{D} = -\begin{pmatrix} \dfrac{\partial u}{\partial r} & -2\dfrac{v}{r} & \dfrac{\partial u}{\partial z} \\ \dfrac{\partial v}{\partial r} + \dfrac{v}{r} & \dfrac{u}{r} & \dfrac{\partial v}{\partial z} \\ \dfrac{\partial w}{\partial r} & 0 & \dfrac{\partial w}{\partial z} \end{pmatrix}$$

Note that if the similarity assumption were valid, i.e. $(u, v, w) = (rf(z), rg(z), h(z))$ with $2f + h' = 0$, this production tensor would reduce to

$$\mathscr{D} = \begin{pmatrix} -f & 2g & -rf' \\ -2g & -f & -rg' \\ 0 & 0 & -h' \end{pmatrix}$$

The similarity profiles (f, g, h) for the boundary layer regime investigated here display two boundary layers of thickness $Re_H^{-1/2}$ on each side of a rotating core in which f is identically zero and g is equal to 0.31. The maximum numerical values for f and h are 0.15 and 0.06, respectively. Examination of the velocity amplitudes in the closed cavity shows that their characteristic numerical values do not depart much from these similarity values, except perhaps in the vicinity of the outer shroud. The dominant terms in the production tensor are thus the axial gradients of the mean flow ($\partial u/\partial z$, $\partial v/\partial z$, $\partial w/\partial z$), which scale as $0.15(r/H)Re_H^{1/2}$, $(r/H)Re_H^{1/2}$, and $6\times 10^{-2}Re_H^{1/2}$, respectively. [2] The largest of these three terms is thus $\partial v/\partial z$, which is almost five times larger than $\partial u/\partial z$. For a given level of axial velocity fluctuations w', the radial and azimuthal velocity fluctuations u' and v' present growth rates of ratio 5 approximately and this accounts for the fact that the azimuthal velocity fluctuations outweigh the radial and axial fluctuations. Likewise the production terms for the Reynolds stress tensor, (i.e. $\mathscr{D}\cdot\mathscr{R} + \mathscr{R}^t\cdot\mathscr{D}^t$ where $\mathscr{R}$ is the symmetrical Reynolds stress tensor) involve the same gradient of the mean flow and its transpose. Allowing for non-axisymmetrical instantaneous fluctuations would not alter these linear growth rates. It would however allow for 3D linear instabilities and some 3D physical mechanisms to take place, such as velocity/pressure gradient correlations. The latter mechanism would redistribute the diagonal Reynolds stress normal to the rotor and stator to the other two tangential diagonal stresses. The axisymmetric assumption does indeed suppress the redistribution towards $\overline{v'^2}$. However the small value of $\overline{w'^2}$ would not change much the ratio between $\overline{v'^2}$ and the other two diagonal stresses, and merely affect the balance between $\overline{u'^2}$ and $\overline{w'^2}$.

A further confirmation of the validity of the above procedure is provided by comparisons with the experimental results presented by Cheah et al. (1994). As already said, these results were obtained in a cavity of $G = 0.127$ and $s = 0$. The peripheral shroud is attached to the stator. The Reynolds number Re_H is set to 4838.7 ($Re_\theta = 3 \times 10^5$). The numbers of grid points in the radial and axial directions (set to satisfy criteria on the smallest resolvable scales) are respectively 2813 and 193. This configuration represents a very severe test due to the strong asymmetry between the rotor and stator boundary layers. Cheah et al. (1994) provided only mean

[2] More precisely $\partial v/\partial z$ scales like $0.7(r/H)Re_H^{1/2}$ and $0.3(r/H)Re_H^{1/2}$ in the stator and rotor boundary layers respectively.

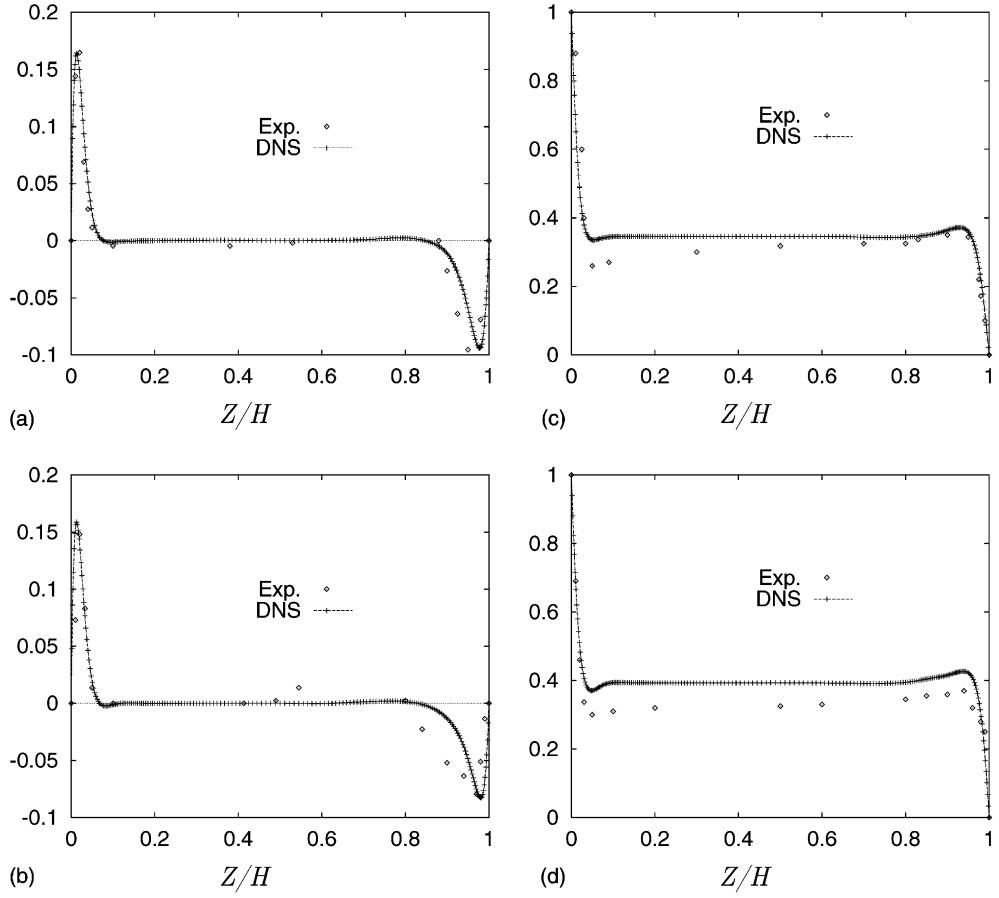

Fig. 2. Comparison with experiment (cavity of Cheah et al.: $G = 0.127$, $s = 0$, $Re_H = 4838.7$ ($Re_\theta = 3 \times 10^5$)): axial distribution (from the rotor ($z = 0$) to the stator ($z = 1$)) of the velocity components ((a) $U/H\Omega$, $R/R_2 = 0.4$; (b) $U/H\Omega$, $R/R_2 = 0.8$; (c) $V/H\Omega$, $R/R_2 = 0.4$; (d) $V/H\Omega$, $R/R_2 = 0.8$).

quantities and we computed these mean quantities from our unsteady simulations using a time averaging technique. Let us just point out that to ensure accurate means, it was found necessary to integrate the equations long enough to reach the asymptotic flow regime before starting the time averaging procedure. In this case, the equations were first integrated over more than 100 disk rotation periods (that is approximately 10^6 time steps starting from an initial condition corresponding to a solution already in the chaotic regime) and time averaging was performed on approximately the same time interval. The averaged fields are obtained from 30 000 samples taken every 40 time steps. It was found necessary to use that many time steps to ensure being in the asymptotic regime and to obtain reliable averages.

Fig. 2 presents radial and azimuthal mean velocity profiles at two radial locations. As can be seen, the general agreement is good. The radial velocity profiles indeed show an excellent agreement in the rotor boundary layer, which is still laminar, and good amplitudes and trends in the stator boundary layer although the boundary layer thickness at $R/R_2 = 0.8$ is underestimated. Concerning the azimuthal velocity components, the profiles in both boundary layers are in good agreement. The main discrepancy lies in the angular rotational velocity of the core which is overpredicted (10%) by the numerical simulations at the largest radial position. This is probably a major consequence of the axisymmetry assumption since it is very likely that allowing for 3D effects would allow for an earlier transition in the *stator* boundary layer and thus reduce the average core angular velocity. [3]

A deeper insight in this confrontation is given by the comparison of the spatial distribution of some Reynolds stresses. Fig. 3 presents comparisons of the azimuthal and axial diagonal turbulence intensities and of the axial–azimuthal component of the stress tensor at a radial position $R/R_2 = 0.8$. As can be seen the amplitudes and shapes are in excellent agreement in the stator boundary layer. The major discrepancy lies on the rotor side, which is found turbulent in the experiments and com-

[3] An upstream shift of the location of the transition point in the stator boundary layer is enough to explain this effect. This point will be made clearer while examining the evolution of the core angular velocity for configuration 1 corresponding to Fig. 8.

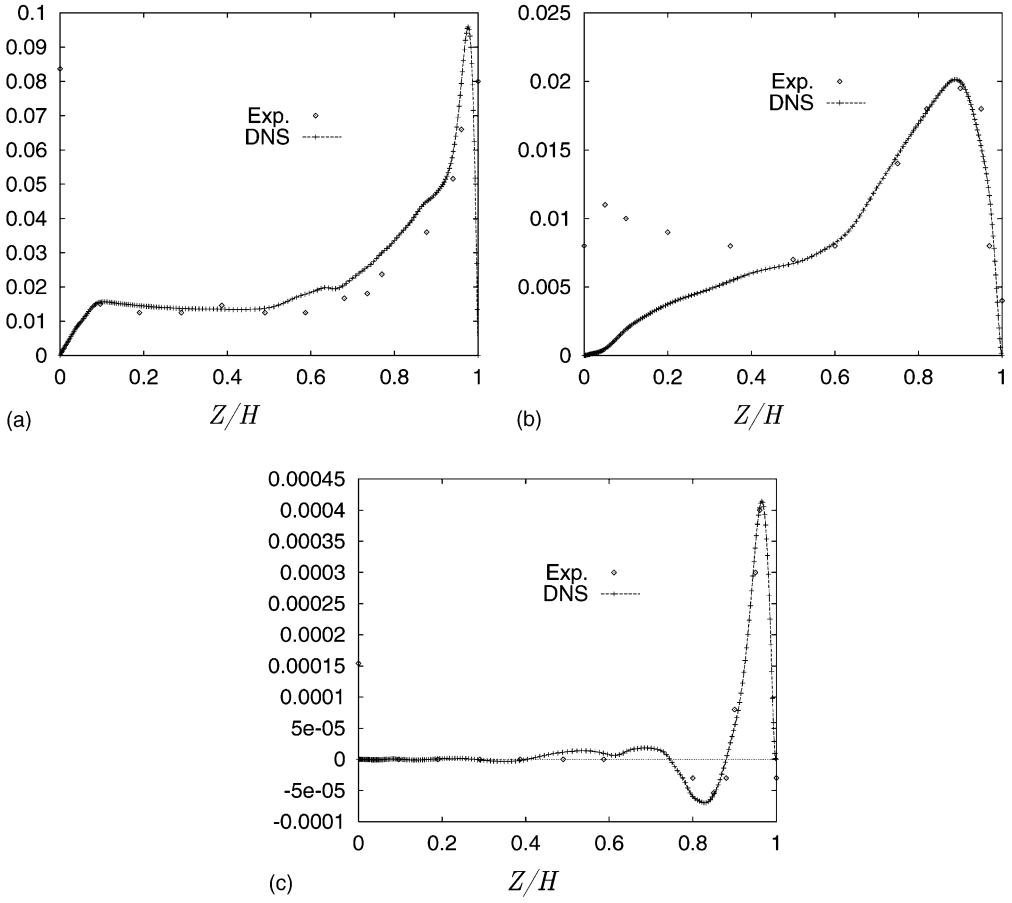

Fig. 3. Comparison with experiment (cavity of Cheah: $G = 0.127$, $s = 0$, $Re_H = 4838.7$ ($Re_\theta = 3 \times 10^5$)): axial distributions of some Reynolds stresses components at the radial location $R/R_2 = 0.8$ (a) $\overline{V'V'}/(R\Omega)^2$, (b) $\overline{W'W'}/(R\Omega)^2$, (c) $\overline{V'W'}/(R\Omega)^2$.

pletely laminar in our simulations. For the experiment, the transition point seems then to be located in the rotor boundary layer, whereas it is located in the stator boundary layer for the computations. We note however that the large turbulence intensity in the experimental results along the rotor seems in contradiction with the mean experimental profiles displayed above, which indeed display the characteristic shape of a laminar rotor boundary layer. This also seems to contradict the generally assumed result (Itoh et al., 1990) that transition in the rotor boundary layer takes place at a local radial rotational Reynolds number Re_r of 3.5×10^5, i.e. above the present value.

Lastly, a further argument that could support the validity of the axisymmetric assumption would lie in the deviation of the turbulence from an axisymmetric behavior. A measure of the state of turbulence is given by Lumley's realisability diagram (Lumley and Newman, 1977) as a function of the invariants of the anisotropy tensor. Given the good agreement between our results and the experimental values for the Reynolds stresses, we have used these values to determine the second and third invariants of the anisotropy tensor. Our representative points fall right on the axisymmetric borderline, an obvious conclusion indeed given the assumption of axisymmetry. Independent results, computed by Elena (1994) from second order Reynolds stress modelling, have however indicated that the corresponding turbulence is not far from the axisymmetric border, which obviously partially supports the assumption of axisymmetry.

The above comparisons have shown that the present numerical simulations, performed under the assumption of axisymmetry, result in satisfactory predictions of the mean and second order moments of the flow. We have supported these observations by a discussion which points on the specific characteristics of these flows by comparison with 2D planar flows. Although computations of rotating flows under the assumption of axisymmetry inevitably miss some phenomenological features, we conclude from the above comparisons and discussions that they cannot be boldly rejected and that they may indeed produce some useful results, at least in the transitional regime investigated here. This could however not hold any longer in the fully developed turbulent regime.

4. Results

The results to be presented below are obtained in the first cavity characterized by $G = 0.125$ and $s = 0.25$. The inner hub and peripheral shroud are attached to the stator. Solutions were computed for a wide range of rotational Reynolds numbers from 10^2 to 10^6. This encompasses the steady laminar regime up to a fully chaotic regime. These results extend the range of Reynolds numbers achieved in the axisymmetric simulations of Randriamampianina et al. (1997), ($Re_\theta < 2.5 \times 10^5$). The flow was found steady for Reynolds numbers smaller than $Re_H = 1300$ ($Re_\theta = 8.3 \times 10^4$). For Reynolds numbers $Re_H \geqslant 200$ ($Re_\theta = 1.3 \times 10^4$) the flow displays a Batchelor type structure consisting of two boundary layers on each side of a core region where the radial velocity is negligible. The thickness of these boundary layers scales like $1/\sqrt{Re_H}$. It is noted however that this solution differs from the usual similarity solution. This can be seen in the radial distribution of the contours of v (see Fig. 4(a)) which are not equally spaced with r as should be the case if the similarity solution were valid (see also the radial distribution of $\overline{V}/R\Omega$ on Fig. 8). Transition to unsteadiness is located for $Re_H = 1370$ ($Re_\theta \approx 8.7 \times 10^4$). It is characterized by mono-periodic oscillations which have their maximum amplitude in the stator boundary layer, close to the inner hub. The characteristic fundamental period is close to 3/4 of a disk rotation period. These oscillations are due to travelling waves which propagate downstream through the stator boundary layer (from the peripheral to the inner hub, see Fig. 4). For the sake of brevity, we do not discuss any further this periodic solution here, which will be presented in more detail elsewhere. Recent

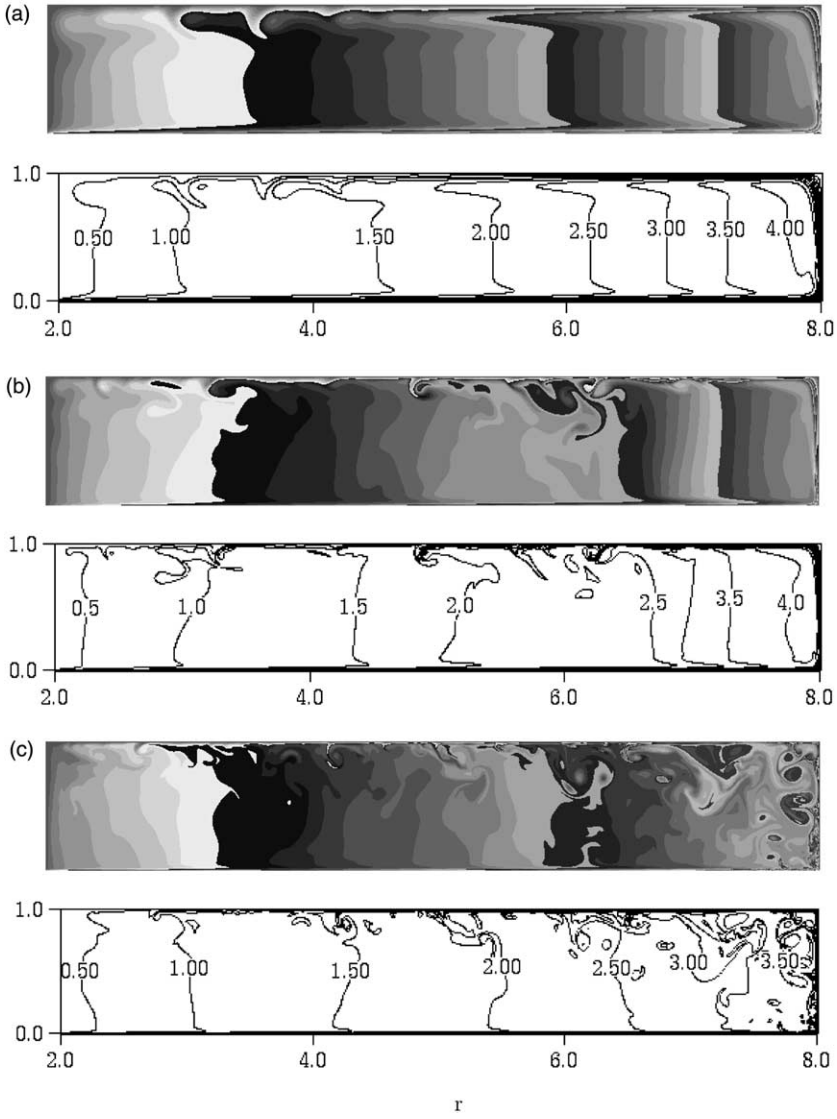

Fig. 4. Instantaneous spatial distributions of the azimuthal velocity component ($V/H\Omega$) for $Re_H = 1500$ (a), $Re_H = 5000$ (b), and $Re_H = 15625$ (c); cavity CV1 (stator is on the top (1) and rotor is downside (0)).

experimental observations have shown that, in the range of aspect ratios considered here, the first instability is indeed axisymmetric (Schouveiler, 1998).

4.1. Instantaneous flow characteristics

For $Re_H > 1500$ ($Re_\theta \approx 10^5$) the flow becomes chaotic. The asymmetry which is observed at the onset of unsteadiness persists over the whole range of Reynolds numbers that were considered. The flow displays fluctuations of much larger amplitude in the stator boundary layer than in the rotor boundary layer. This feature is characteristic of these rotor–stator cavities. It is amplified in our particular case due to the boundary conditions we have considered on the inner and outer shrouds. Indeed, the stationary inner hub helps to relaminarize the flow whereas the flow is destabilized along the stationary outer shroud. We have obtained asymptotic chaotic solutions for two values of the Reynolds number, $Re_H = 5000$ ($Re_\theta = 3 \times 10^5$) and $Re_H = 15\,625$ ($Re_\theta = 10^6$). Typical visualizations of the azimuthal velocity component field are displayed in Fig. 4. As can be seen, the solution for $Re_H = 5000$ is still in the transitional regime, whereas that for $Re_H = 15\,625$ exhibits a fully turbulent region close to the peripheral shroud.

The solution for $Re_H = 5000$ is characterized by the intermittent ejection of large eddies, the size of which is approximatively $1/5$ of the cavity height. After their ejection these eddies generally quickly dissipate. Time traces of the azimuthal velocity component taken at different locations are displayed in Fig. 5. As can be seen, the monitoring points located in the stator boundary layer exhibit fluctuations of high frequency. The frequency decreases as the location of the monitoring point moves downstream through the stator boundary layer (from the peripheral shroud to the inner hub). The amplitude of the oscillations is very large, of the same order as the mean velocity, and the relative amplitude of the oscillations thus remains approximately constant with the local radius. It is also apparent that the signal taken at a location close to the stator and in the upstream part of the stator boundary layer (see Fig. 5(a), $R/R_2 = 0.8$ and $Z/H = 0.9$) is very asymmetric, the fluctuations above the mean being of smaller amplitude than those below the mean. At points located farther downstream at the same distance from the stator (at $Z/H = 0.9$ and $R/R_2 = 0.375$), the fluctuations above and below the mean are approximately symmetrical around the mean. These different behaviors are explained by the change of relative location of the points with respect to the boundary layer thickness since the boundary layer becomes turbulent as it proceeds downstream. The upstream point is indeed located on the outer part of the boundary layer and the presence of the rotating core thus prevents large fluctuations above the mean. The point located downstream, although at the same distance from the stator, is now fully in the boundary layer and the presence of the core is felt less.

On the other hand time traces at monitoring points located in the core region or in the rotor boundary layer display fluctuations of much lower frequency. The visualization of a set of instantaneous spatial distributions of the azimuthal velocity shows that the fluctuations in the core are characterized by periodic oscillations of the isovalues of the azimuthal velocity in the axial direction. These oscillations are attributed to inertial wave oscillations which are kept permanently excited by the large eddies ejected from the stator boundary layer. It is known that these inertial waves constitute a solution of the Navier–Stokes equation in a fluid rotating as a solid body (Lighthill, 1979). In this case, the dispersion relationship of these waves reads: $\omega = 2 \times \Omega_0 \cos(\theta)$, where ω represents the pulsation of the inertial waves, Ω_0 the rotational velocity of the fluid, and θ the angle between the axis of rotation and the waveplanes (constant phase planes). The dominant dimensionless pulsation of the oscillations in the core region is almost twice the angular rotational velocity of the core at a given radius. This dominant frequency increases slightly with the radial location, at the same rate as does the angular velocity of the core. To isolate the spatial structure of these low frequency oscillations for $Re_H = 5000$, we have made a Fourier analysis of a sample of instantaneous spatial distributions of the azimuthal velocity. We have kept the low frequency component by applying a filter centered around the dimensionless pulsation 0.8 (which corresponds to the dominant low frequency in the region $0.6 < R/R_2 < 0.9$) and transformed the filtered spatial distributions back into physical space. Examination of the time evolution of the corresponding distributions indeed shows that these structures are travelling axially from the stator to the rotor boundary layer (see Fig. 6). The waveplanes are thus almost normal to the rotation axis ($\theta \simeq \pi/2$) which is consistent with the dispersion relationship. The measured wavelength λ is $\lambda \simeq 2H/3$. A further characterization of these inertial waves is given by the comparison of the phase velocity of the fluctuations to the phase velocity of the inertial waves given by the dispersion relationship $V_\phi = (\lambda\Omega_0/2\pi)\sin(\theta)$ which are both equal to $V_\phi/H\Omega \simeq 0.17$.

For $Re_H = 15\,625$, the most distinctive feature is that the boundary layer along the rotor becomes unstable in its most downstream part (i.e. $R/R_2 \geqslant 0.8$, see also Fig. 10(b)). This, in conjunction with the destabilizing effect of the stationary outer shroud, results in a very turbulent region that fills the entire clearance for $R/R_2 \geqslant 0.8$. This region is characterized by eddies of size between $H/3$ and $H/20$. The larger eddies may consist of dipoles which, once formed, move quickly in the core and may impinge on the rotor boundary layer. This impingement squeezes the rotor boundary layer and triggers waves

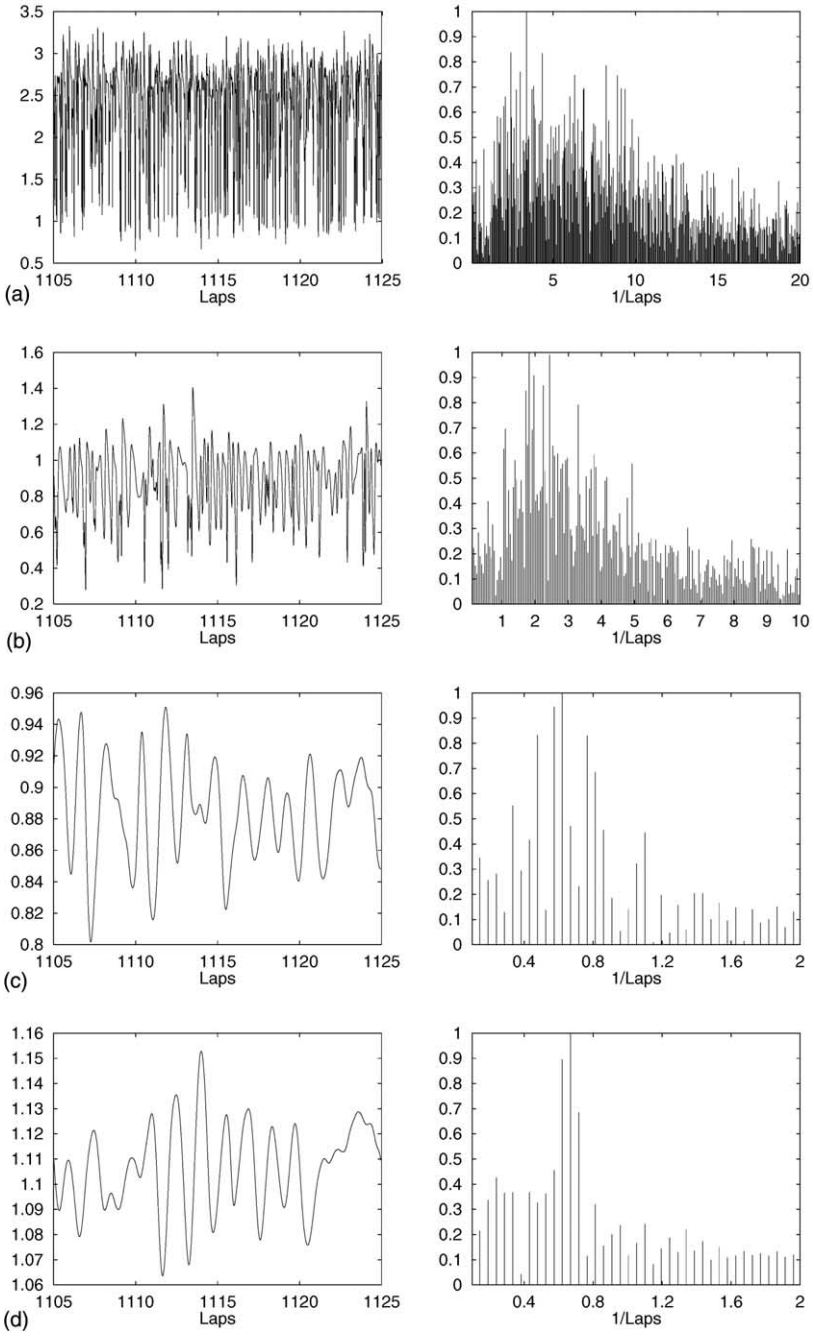

Fig. 5. Time traces (time unit in laps) and corresponding density power spectra of the azimuthal velocity component ($V/H\Omega$), (a) stator boundary layer ($R/R_2 = 0.8$, $Z/H = 0.9$), (b) stator boundary layer ($R/R_2 = 0.375$, $Z/H = 0.9$), (c) core region ($R/R_2 = 0.375$, $Z/H = 0.5$), (d) rotor boundary layer ($R/R_2 = 0.375$, $Z/H = 0.1$); cavity CV1, $Re_H = 5000$ ($Re_\theta = 3 \times 10^5$).

which propagate downstream. All these phenomena are very intermittent, especially in the rotor boundary layer. As a consequence, the core region close to the external shroud becomes much more homogeneous, as will be seen in more detail below. Inertial waves are still present in the core region closer to the inner hub, as can be seen from Fig. 4, and from power spectra of time traces in the core region which are not displayed for the sake of brevity. The value of the local Reynolds number at which travelling waves are observed in the rotor boundary layer is approximately 4×10^5, corresponding to $R/R_2 \simeq 0.8$. This value is in good agreement with values generally quoted in the literature. Let us however emphasize that we believe that this instability is not intrinsic, but results from the exterior perturbations of the large eddies ejected from the external shroud or from the stator boundary layer. These precise effects could of course be largely due to the assumption of

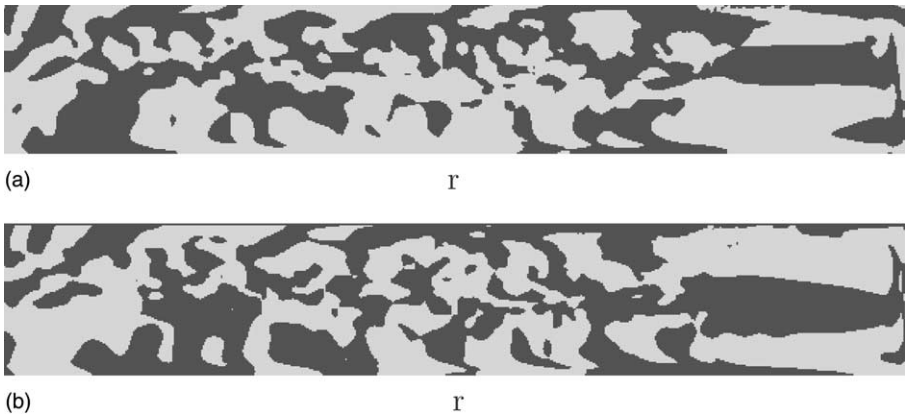

Fig. 6. Two instantaneous spatial distributions of the fluctuations associated to the inertial waves, at t_0 (a) and $t_0 + \Delta t$ (b) (Δt corresponds to an half disk rotation period). The frequency filter is centered around the dominant low frequency in the core in the last part of the cavity ($0.75 < R/R_2 < 0.9$). The fluctuations travel axially from the stator boundary layer to the rotor boundary layer.

axisymmetry and might not hold for fully three-dimensional flows.

4.2. Turbulence statistics

Time averaged first and second order moments were computed for the two values of the Reynolds numbers already presented ($Re_H = 5000$ and 15 625). As previously discussed, care was taken to integrate long enough in time to ensure accurate evaluations of these first- and second-order moments. Accurate third-order moments were also obtained for $Re_H = 5000$.

4.2.1. Mean flow structure

Time averaged azimuthal velocity fields are presented in Fig. 7. To a first-order approximation, they display the usual flow structure characteristic of the Batchelor type discussed earlier. In particular, both fields show the existence of a well-defined core region characterized by zero radial velocity and local rigid body rotation. These mean flows were obtained after averaging every 30 time steps (time step value of 6×10^{-4} for $Re_H = 5000$ ($Re_\theta = 3 \times 10^5$), and 2×10^{-4} for $Re_H = 15\,625$ ($Re_\theta = 10^6$)) over time lengths corresponding to respectively 500 and 20 disk rotation periods. The small wiggles still present in the solution for $Re_H = 15\,625$ confirm that it is indeed necessary to integrate the equations for this long to smooth out the large instantaneous eddies present in the unsteady solution and to obtain accurate mean values. Let us also emphasize that it requires less time averaging for the highest value of the Reynolds number, but of course more cpu time due to the increased spatial resolution and smaller time step value. This is due to the fact that the solution for the largest Reynolds number is more turbulent than for the lowest one, which results in an increased mixing and hence shorter times to average out the unsteady features.

A closer look at the solution shows however that the mean flow structure has started to depart significantly from the asymptotic flow structure corresponding to the end of the steady laminar regime. This is particularly visible in the radial profiles of the core swirl ratio ($V/R\Omega$) displayed in Fig. 8. The curves corresponding to the two largest values of the Reynolds number increasingly differ from those obtained for the other three lower Reynolds numbers (corresponding to laminar flow regime) at values of $R/R_2 > 0.7$, except that for $Re_H = 5000$ which matches the other three very close to the outer shroud. The rather large differences in the curves corresponding to the beginning of the unsteady regime also show the sensitivity of this parameter to the local characteristics of the stator boundary layer, as already pointed out by Morse (1991). It appears furthermore that the radial distribution of the rotational velocity of the core exhibits a sharp decrease when transition occurs in the stator boundary layer (the location of the transition is $r/R_2 \simeq 0.55$ for $Re_H = 1500$ ($Re_\theta \approx 10^5$) and $r/R_2 \simeq 0.8$ for $Re_H = 5000$ ($Re_\theta = 3 \times 10^5$) on Fig. 8). The radial location of this decrease confirms that the transition point moves upstream (first from the middle part of the cavity to the peripheral shroud) in the stator boundary layer when the Reynolds number increases. It also confirms the great sensitivity of the core angular velocity to the location of the transition in the stator boundary layer.

At the highest Reynolds number, the swirl ratio no longer exhibits such a decrease since the transition point has moved to the boundary layer on the peripheral shroud or in the top part of the rotor boundary layer. Furthermore, this ratio increases from 0.35 close to the inner hub to 0.4 approximately in the outer region. This evolution is probably linked to the unsteadiness in the rotor boundary layer in its most downstream part, as reported by others (Cheah et al., 1994). Thus,

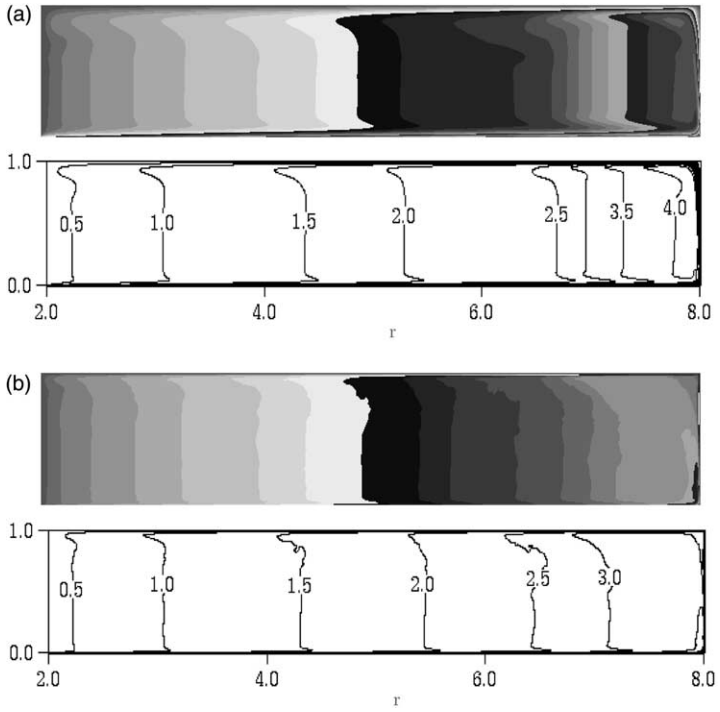

Fig. 7. Spatial distribution of the averaged azimuthal velocity component ($\overline{V}/H\Omega$) for $Re_H = 5000$ (a) and $Re_H = 15625$ (b); cavity CV1 (stator is on the top (1) and rotor is downside (0)).

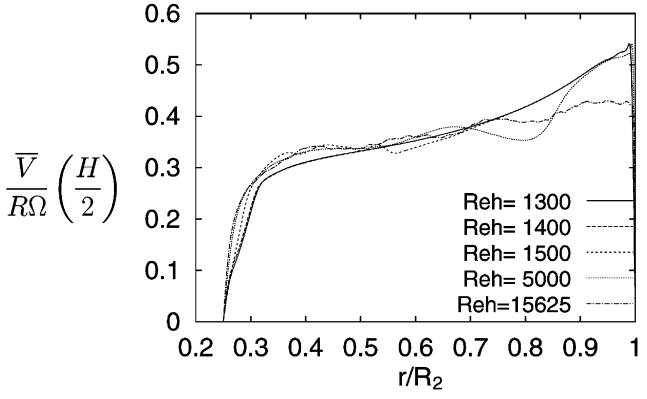

Fig. 8. Radial distribution of the angular rotational velocity of the core ($(\overline{V}/R\Omega)(H/2)$) for five Reynolds numbers: $Re_H = 1300$ ($Re_\theta = 8.3\times 10^4$, stationary solution), $Re_H = 1400$ ($Re_\theta = 8.9 \times 10^4$, mono-periodic oscillatory solution), $Re_H = 1500$ ($Re_\theta = 9.6 \times 10^4$, transitional solution), $Re_H = 5000$ ($Re_\theta = 3 \times 10^5$, partially turbulent stator boundary layer), and $Re_H = 15625$ ($Re_\theta = 10^6$, the stator and peripherical shroud boundary layers are turbulent); cavity CV1.

paradoxically enough, the swirl ratio in the core for $Re_H = 15625$ departs less from the value for the similarity solution than for smaller Reynolds values.

One quantity of primary importance for engineering applications is the torque transmitted from the rotor to the stator. This quantity has been the object of many investigations and correlations have long been established valid for specific flow regimes (Daily and Nece, 1960). The correlations for the two regimes characterized by separated boundary layers usually referred to as II and IV (Owen and Rogers, 1989) (regime II is laminar and IV is turbulent) are $C_m = 1.85G^{1/10}Re_\theta^{-1/2}$ and $C_m = 0.051G^{1/10}Re_\theta^{-1/5}$ respectively. The first four rows of Table 2 summarize our findings in configuration CV1 compared to the above correlations in the appropriate flow regime. It can be seen that the agreement, although generally good, is better in the turbulent than in the laminar regime. The last two lines present similar comparisons for the geometrical configuration without the inner hub. As can be seen the agreement is now much better in the laminar regime, and the differences observed for the first geometrical configurations can thus be ascribed to the difference in boundary conditions on the inner hub (the correlations proposed by Daily and Nece (1960) were established for a rotating inner hub).

Table 2
Torque coefficient on the rotor

Reynolds number	Computations	Correlations
$Re_H = 1300$ (II)	6.7×10^{-3}	5.2×10^{-3}
$Re_H = 1500$ (II)	6.3×10^{-3}	4.9×10^{-3}
$Re_H = 5000$ (IV)	3.5×10^{-3}	3.3×10^{-3}
$Re_H = 15625$ (IV)	2.4×10^{-3}	2.6×10^{-3}
$Re_H = 1440$ (Cheah-II)	4.6×10^{-3}	4.7×10^{-3}
$Re_H = 4838$ (Cheah-IV)	2.7×10^{-3}	2.7×10^{-3}

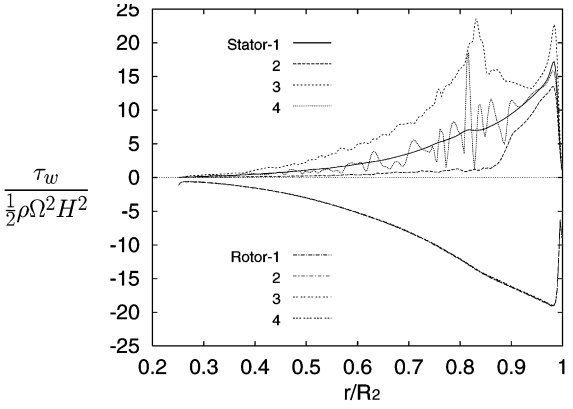

Fig. 9. Radial distribution of the local wall shear stress ($\tau_w/(1/2)\rho\Omega^2H^2$) for $Re_H = 5000$ ($Re_\theta = 3 \times 10^5$). The curves for the stator (resp. rotor) side are plotted as positive (resp. negative) values. 1: average distribution, 2: minimum envelope, 3: maximum envelope, 4: instantaneous distribution; cavity CV1.

In addition to these mean values, the axisymmetric numerical simulations give access to the space and time dependence of the wall shear stress coefficient. Fig. 9 presents several radial distributions of this quantity both on the rotor and on the stator. These different curves correspond to the time averaged distribution, a typical instantaneous distribution and the maximum and minimum envelopes in time of the instantaneous distribution. As can be seen all four curves cannot be distinguished for the rotor side, which confirms, if still needed, the steady character of the rotor boundary layer. On the other hand, these curves are widely separated along the stator side, indicating fluctuations of large amplitude. Starting from the upstream corner, the distance between lower and upper envelopes increases at first in the transition region, corresponding to the amplification of the travelling waves, reaches a maximum around $R/R_2 = 0.8$ where the turbulence intensity is maximum, and then steadily decreases further downstream. It can be also seen that the fluctuations above the mean are of larger amplitude than those below the mean, indicating a non-gaussian probability distribution.

4.2.2. Second-order moments

All second-order moments were computed for both Reynolds values of $Re_H = 5000$ and 15 625. To start this presentation, Fig. 10 displays the fields of turbulent kinetic energy determined for both Reynolds numbers. As can be seen these fields are consistent with the phenomenology already described. At the lower Reynolds number the turbulent kinetic energy is maximum in the stator boundary layer at around $R/R_2 \simeq 0.8$, whereas for the largest value of the Reynolds number, the location of the maximum is shifted to the downstream part of the rotor boundary layer, just before the corner between the rotor boundary layer and the outer shroud. Note that for $Re_H = 15\,625$, the secondary maximum in the stator boundary layer found at $R/R_2 = 0.85$ is three times smaller than the maximum value. This means that when the rotor boundary layer becomes turbulent it is characterized by turbulence intensities much larger than those found along the stator. Similar behavior has been reported either experimentally (Cheah et al., 1994) or numerically (Randriamampianina et al., 1997).

Axial profiles (from the rotor to the stator) of the components of the Reynolds stress tensor at one radial location corresponding to the maximum of turbulent kinetic energy found for $Re_H = 5000$ (i.e. $R/R_2 = 0.8$) are displayed in Figs. 11 and 12. These quantities are displayed using two different scalings. In Fig. 11, the values $\overline{U_i'U_j'}$ are scaled with $(R\Omega)^2$ whereas in Fig. 12 they are scaled using the modulus of the friction velocity in each boundary boundary layer, which explains the discontinuity at $z = 1/2$. These scalings have been used in Cheah et al. (1994) and Itoh et al. (1990) respectively.

Fig. 11 shows that the dominant contribution to the turbulent kinetic energy comes from the azimuthal component which is 8–10 times larger than the contributions from the radial or axial components. When scaled using the friction velocity (Fig. 12), the profiles of these turbulent intensities for both Reynolds numbers at the location corresponding to the maximum of the turbulence intensity in the stator boundary layer exhibit striking similarities, both in amplitude and in shape. Locations of the maximum of the turbulence intensities for the radial and azimuthal velocity components are found at a distance of approximately 15 wall units, in agreement with the results of Itoh. The maximum for the axial component is located approximately 10 times further away from the wall. These similarities between the normalized Reynolds stress distributions for both Reynolds numbers are somewhat surprising since one might think that the flows corresponding to these two Reynolds numbers would not pertain to the same flow regime and their turbulence characteristics would scale differently.

4.2.3. Kinetic energy budgets

A kinetic energy budget was computed for the Reynolds number value of 5000 ($Re_\theta = 3 \times 10^5$), in the stator boundary layer at $R/R_2 = 0.8$ (Fig. 13). As said earlier, the computation of such a budget requires the computation of the third order moments, which implies very long integration times. A good test of the accuracy of such a computation is to compute the balance which should be close to zero. We have also checked the validity of the kinematic relationship between the turbulent kinetic energy and the viscous dissipation rate ($\epsilon = 2\nu(\partial\sqrt{\kappa}/\partial N)^2$ or $\epsilon = \nu(\partial^2\kappa/\partial N^2)$) at the wall, which is an indication that enough resolution was used within

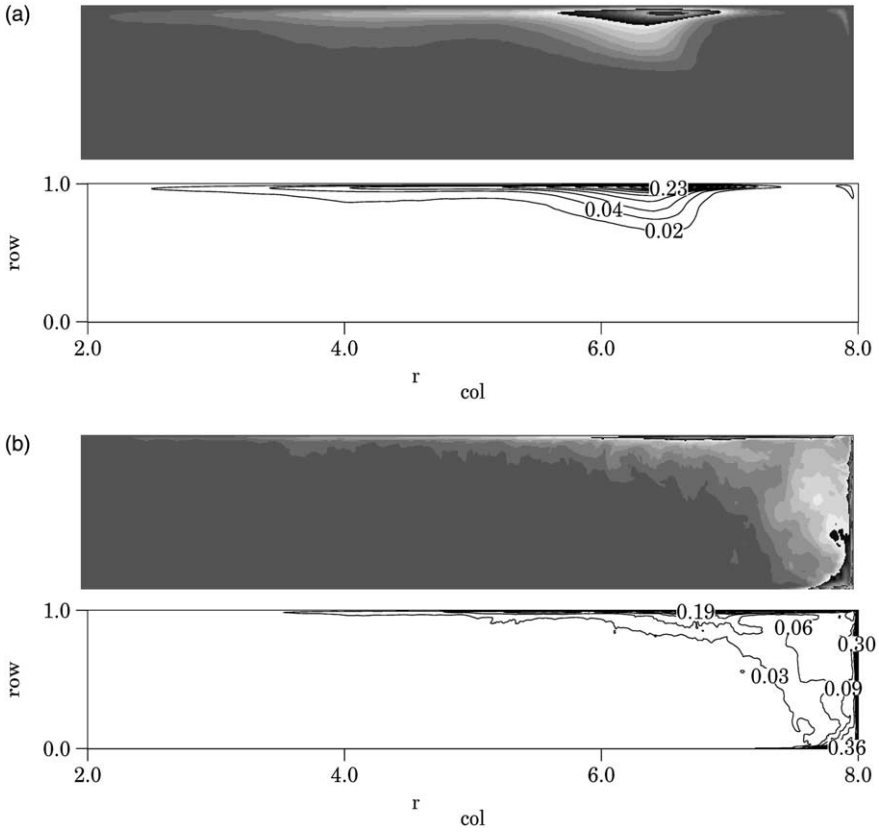

Fig. 10. Spatial distribution of the turbulent kinetic energy ($\kappa/H^2\Omega^2$) for $Re_H = 5000$ ($Re_\theta = 3 \times 10^5$) (a) and $Re_H = 15625$ ($Re_\theta = 10^6$) (b). The maximum value of the turbulent kinetic energy at $Re_H = 15625$ is twice that for $Re_H = 5000$; cavity CV1 (stator is on the top (1) and rotor is downside (0)).

the viscous sublayer (we have checked the second form which is more demanding numerically).

This kinetic energy budget exhibits some similarities with those corresponding to other types of flows, but presents some peculiar features due likely to rotation effects. The general trends exhibited by all the terms in the budget are similar to those found in channel flows (see e.g. Eggels et al., 1994). In particular the maximum of the production is located at $y^+ \sim 20$. It is noted however that the production rate of the turbulent kinetic energy goes to zero in the core region, which is due to the vanishing of the gradient of the mean flow, and to the quasi-linear radial variation of the azimuthal velocity component in the core.

Out of the viscous sublayer, the budget does show some specific features. In particular, the turbulent diffusion is larger than the velocity–pressure correlation or the viscous diffusion, a trend which differs from the evolution observed in channel flows or along flat plates. Indeed, the turbulent diffusion plays a major role in the log-law region by balancing the production term, a role which is classically devoted to the viscous dissipation which in this case accounts only for 50% of the total loss term. The important role of turbulent diffusion has obviously to be linked to the low level of the viscous dissipation rate. Does this come from the assumption of axisymmetry, which indeed suppresses the azimuthal contribution or does it come from rotation effects, as was pointed out in some theoretical and experimental studies? Experimental (Ibbetson and Tritton, 1975) or numerical studies (Cambon and Jacquin, 1989; Bardina et al., 1985) of a damped turbulence submitted to rotation, have indeed reported an inhibition of the energy transfer from small to high wavenumbers which results in a reduction of the viscous dissipation rate. It is thus hard to say now if the assumption of axisymmetry we have used is responsible for the increased role of turbulent diffusion, or if this is due to rotation effects alone.

The inertial waves in the core are another mechanism which can play a role in the turbulent transport. This mechanism is probably complex since: on the one hand, these waves are kept excited by a fraction of the shear production at the wall; on the other hand it has been suggested that they could be responsible for a turbulent transport from the core towards the walls (Ibbetson and Tritton, 1975). The discussion of the instantaneous flow characteristics has shown that the pulsations associated

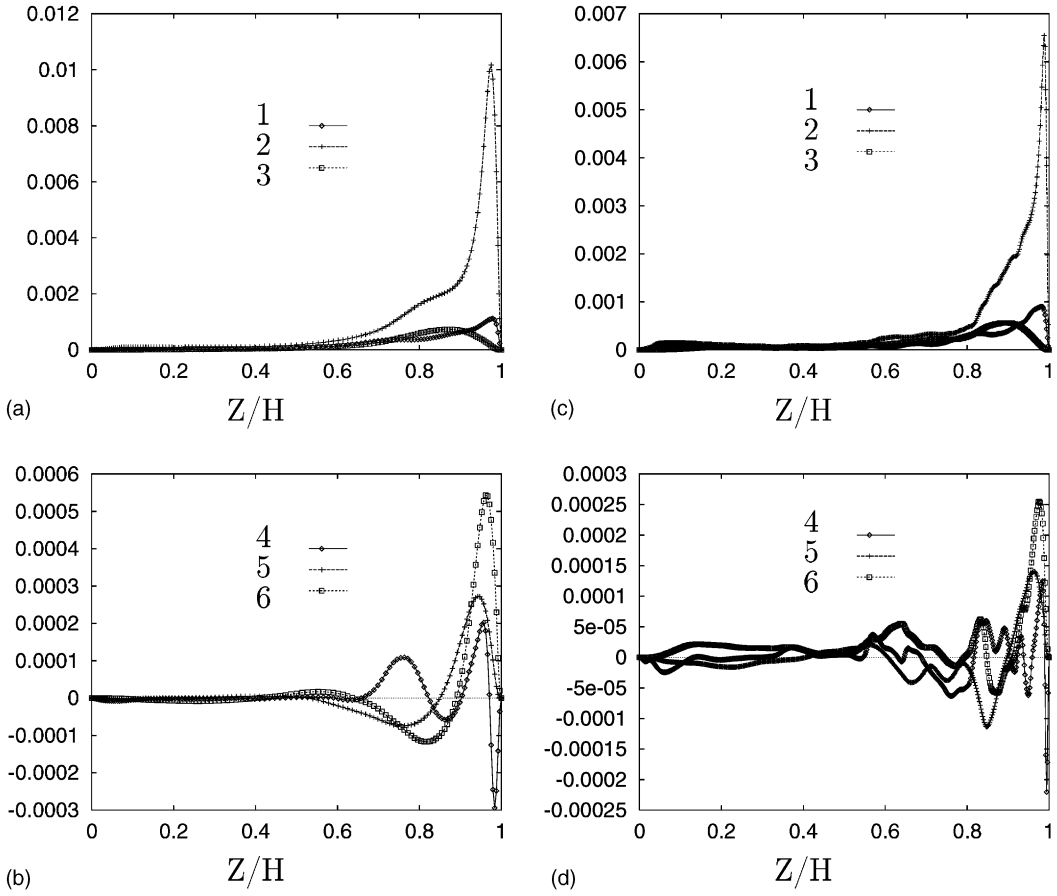

Fig. 11. Reynolds stresses axial distributions normalized by $(R\Omega)^2$ at $R/R_2 = 0.8$. (a,b) diagonal and off diagonal stresses for $Re_H = 5000$ ($Re_\theta = 3 \times 10^5$), (c,d) diagonal and off diagonal stresses for $Re_H = 15625$ ($Re_\theta = 10^6$). (1) $\overline{U'U'}/(R\Omega)^2$, (2) $\overline{V'V'}/(R\Omega)^2$, (3) $\overline{W'W'}/(R\Omega)^2$, (4) $\overline{U'V'}/(R\Omega)^2$, (5) $\overline{U'W'}/(R\Omega)^2$, (6) $\overline{V'W'}/(R\Omega)^2$; cavity CV1. The rotor is located at $Z/H = 0$ and the stator at $Z/H = 1$.

with the inertial waves in the core, are concentrated on the upper bound authorized by the dispersion relationship. This means that these waves are close to mono-chromatic, and therefore could not contribute significantly to any transport of the turbulent energy. Furthermore, the ratio between a time characteristic of these waves ($\tau_{iw} = \left(H^2/\nu\Omega\right)^{1/2}$, Ibbetson and Tritton, 1975), and a time characteristic of the large scales of the turbulence ($\tau_{ls} = \kappa/\epsilon$), is always greater than 10 everywhere in the unsteady part of the flow which would suggest slight influence of the inertial waves on the turbulence.

5. Conclusion

We have performed numerical simulations of turbulent flows in rotor stator cavities using a finite difference algorithm based on a multi-domain decomposition strategy. For cpu limitations, these simulations have been performed under the assumption of axisymmetry. Comparisons with existing experimental data have shown however reasonable agreement, not only for the first-order but also for the second order moments. These simulations have indeed confirmed that the flow becomes first turbulent on the stator while the rotor boundary layer remains completely laminar and that the two boundary layers continue to behave differently at larger Reynolds numbers. In the turbulent regime, we have shown that the large eddies ejected from the stator boundary layer into the core keep the internal waves in the core permanently excited. We have also shown that the local averaged angular rotational velocity of the core is very sensitive to the flow regime. Good agreement was found between the time averaged torque values and experimental correlations. Large deviations in space and time of the local torque coefficient however were found in the stator boundary layer. Good similarity between the distributions of the Reynolds stresses obtained for the two different Reynolds numbers was found. A detailed analysis of the kinetic energy budget has shown the unusual importance of the turbulent diffusion term. Future 3D computations will tell whether this result is generic of turbulent

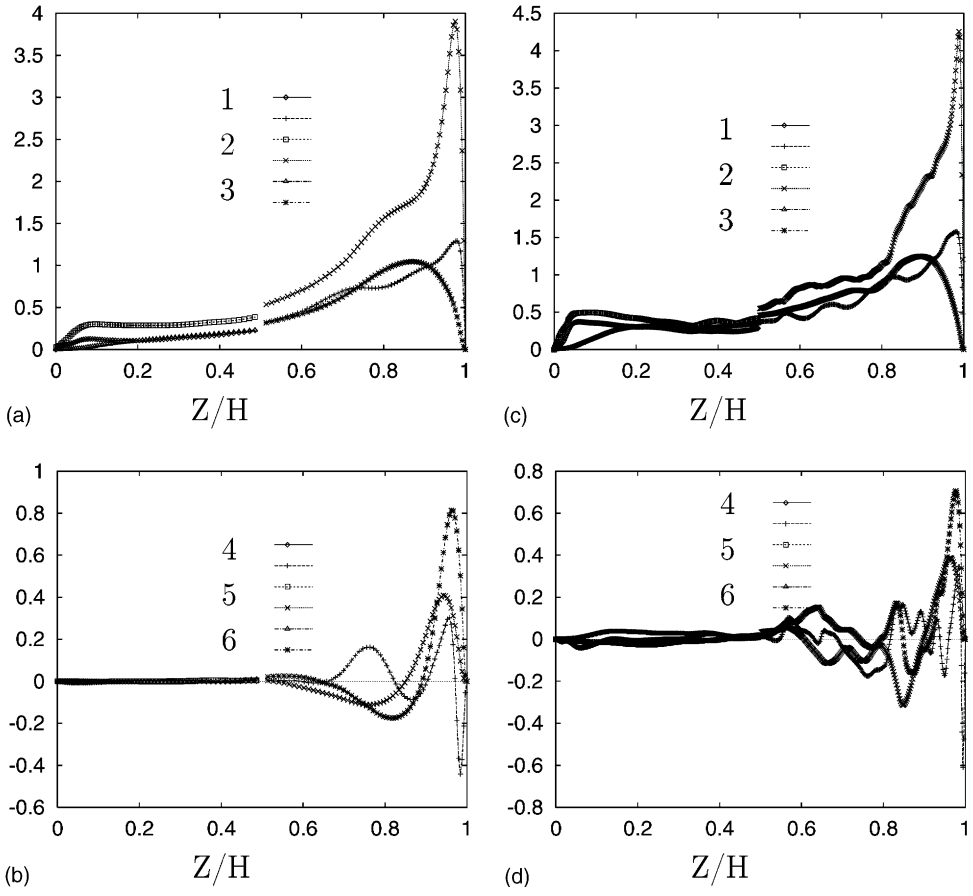

Fig. 12. Reynolds stresses axial distributions at $R/R_2 = 0.8$. The Reynolds stresses are normalized by the friction velocity at the wall (U_τ). (a,b) diagonal and off diagonal stresses for $Re_H = 5000$ ($Re_\theta = 3 \times 10^5$), (c,d) diagonal and off diagonal stresses for $Re_H = 15625$ ($Re_\theta = 10^6$), (1) $\sqrt{\overline{U'U'}}/U_\tau$, (2) $\sqrt{\overline{V'V'}}/U_\tau$, (3) $\sqrt{\overline{W'W'}}/U_\tau$, (4) $\overline{U'V'}/(U_\tau)^2$, (5) $\overline{U'W'}/(U_\tau)^2$, (6) $\overline{V'W'}/(U_\tau)^2$; cavity CV1. The rotor is located at $Z/H = 0$ and the stator at $Z/H = 1$.

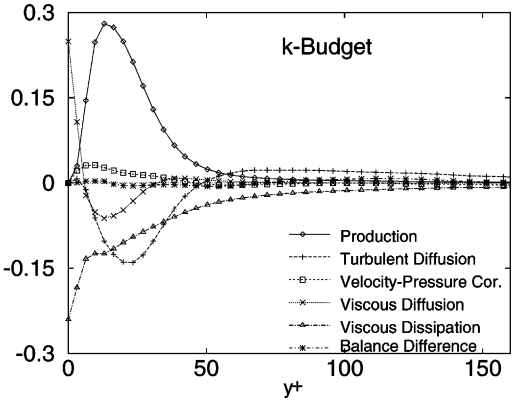

Fig. 13. Turbulent kinetic energy budget in the stator boundary layer at $R/R_2 = 0.8$ for $Re_H = 5000$ ($Re_\theta = 3 \times 10^5$); cavity CV1. The terms are normalized by U_τ^4/ν. Note that the Balance Difference is close to zero, indicating that the errors due to the spatial discretization and time-averaging of the transport equation of the turbulent kinetic energy are small.

rotating flows or mostly due to the assumption of axi-symmetry.

Acknowledgements

The computations were performed of the Cray T3D and T3E of IDRIS. Computing Time was provided through a grant from Scientific Council of IDRIS. This work is part of the Ph.D. work of R. Jacques, who was supported both by CNRS and by SNECMA. We acknowledge many stimulating and helpful discussions with Dr Ch. Tenaud from LIMSI, and with Dr D. Dutoya and Dr E. Laroche from ONERA.

References

Bardina, J., Ferziger, J.H., Rogallo, R.S., 1985. Effect of rotation on isotropic turbulence: computation and modelling. J. Fluid Mech. 154, 321–336.

Cambon, C., Jacquin, L., 1989. Spectral approach to non-isotropic turbulence subjected to rotation. J. Fluid Mech. 202, 295–317.

Cheah, S.C., Iacovides, H., Jackson, D.C., Ji, H., Launder, B.E., 1994. Experimental investigation of enclosed rotor–stator disc flows. J. Exp. Ther. Sci. 9, 445–455.

Chew, J.W., Vaughan, C.M., 1988. Numerical predictions for the flow induced by an enclosed rotating disc. In: Proceedings of the Gas

Turbine and Aeroengine Congress, ASME paper 88-GT-127, Amsterdam, The Netherlands.

Daily, J.W., Nece, R.E., 1960. Chamber dimension effects on induced flow and frictional resistance of enclosed rotating disks. J. Basic Eng. 82, 217–232.

Daube, O., 1992. Resolution of the 2D Navier–Stokes equations in velocity-vorticity form by means of an influence matrix technique. J. Comp. Phys. 103, 402–414.

Eggels, J.G.M., Unger, F., Weiss, M.H., Westerweel, J., Adrian, R.J., Friedrich, R., Nieuwstadt, F.T.M., 1994. Fully developed turbulent pipe flow: a comparison between direct numerical simulation and experiment. J. Fluid Mech. 268, 175–209.

Elena, L., 1994. Modélisation de la turbulence inhomogène en présence de rotation, thèse, University of Aix-Marseille II.

Elena, L., Schiestel, R., 1996. Turbulence modeling of rotating confined flows. Int. J. Heat Fluid Flow 17, 283–289.

Fromm, J., 1987. Understanding turbulence through Navier–Stokes computation of flow between rotating disks. IBM Research Report, RJ 5999 (59598) Mathematics/Physics, IBM Almaden Research Center, 1–31.

Fromm, J., 1988. Computation of turbulent transition in flow between rotating disks. In: de Vahl Davis, G., Fletcher, C. (Eds.), Computational Fluids Dynamics. Elsevier, North Holland, pp. 51–62.

Grötzbach, G., 1983. Spatial resolution requirements for direct numerical simulation of the Rayleigh-Bénard convection. J. Comp. Phys. 49, 241–264.

Iacovides, H., Launder, B.E., 1995. Computational fluid dynamics applied to internal gas-turbine blade cooling: a review. Int. J. Heat Fluid Flow 16, 454–470.

Ibbetson, A., Tritton, D.J., 1975. Experiments on turbulence in a rotating fluid. J. Fluid Mech. 68, 639–672.

Itoh, M., Yamada, Y., Imao, S., Gonda, M., 1990. Experiments on turbulent flow due to an enclosed rotating disk. In: Rodi, W., Ganič, E.N. (Eds.), Proceedings of International Symposium on Engineering Turbulence Modelling and Experiments. Dubrovnik, Yugoslavia, Elsevier Science, New York, pp. 659–668.

Jacques, R., Quéré, P., Daube, O., 1998. Comparaisons entre simulations directes et modélisations k–ϵ pour les écoulements dans une cavité interdisques en configuration rotor–stator. Revue Générale de Thermique 37, 565–581.

Lesieur, M., 1987. Turbulence in Fluids. Kluwer Academic Publishers, Dordrecht.

Lighthill, J., 1979. Waves in Fluids. Cambridge University Press, Cambridge, MA.

Lumley, J.L., Newman, G.R., 1977. The return to isotropy of homogenous turbulence. J. Fluid Mech. 82, 161–178.

Morse, A.P., 1991. Assessment of laminar-turbulent transition in closed disk geometries. J. Turbomachinery 113, 131–138 (Transactions of the ASME).

Nagano, Y., Tagawa, M., Tsuji, T., 1991. Effects of adverse pressure gradients on means flows and turbulence statistics in a boundary layer. In: Proceedings of Eight Symposium on Turbulent shear flows, Technical University of Münich, 2-3-1 2-3-6.

Owen, J.M., Rogers, R.H., 1989. Flow and heat transfer in rotating disc systems. vol. 1: Rotor–Stator Systems. Research Studies Press, UK, Wiley Inc., USA.

Randriamampianina, A., Elena, L., Fontaine, J.P., Schiestel, R., 1997. Numerical prediction of laminar, transitional and turbulent flows in shrouded rotor–stator systems. Phys. Fluids 9–6, 1696–1713.

Ton, F.K., Lin, C.A., 1994. Predictions of turbulent flows between a rotating and a stationary disk. In: Proceedings of Symposium on Turbulent Heat and Mass Transfer, Lisbon, Portugal.

Vanel, J.M., Peyret, R., Bontoux, P., 1986. A pseudo-spectral solution of vorticity-stream function equations using the influence matrix technique. In: Num. Meth. Fluid Dyn. II. Clarendon Press, Oxford, pp. 463–475.

Schouveiler, L., 1998. Sur les instabilités des écoulements entre un disque fixe et un disque en rotation, thèse, University of Aix-Marseille II.